Effective Microbial Kinetics under Pore-Scale Transport Limitation: A Biofilm Effectiveness-Factor Theory

Shahram Asgari

Department of Marine Sciences, University of Georgia, Athens, GA 30602, USA

Email: shahram.asgari@uga.edu

ORCID: 0009-0004-3810-2739

This is a non-peer-reviewed preprint submitted to EarthArXiv. It has not undergone peer review. The manuscript is intended for submission to the peer-reviewed journal Geoscientific Model Development.

Effective Microbial Kinetics under Pore-Scale Transport Limitation: A Biofilm Effectiveness-Factor Theory

Shahram Asgari

Department of Marine Sciences, University of Georgia, Athens, GA 30602, USA

Correspondence: shahram.asgari@uga.edu

Abstract

Reactive-transport models of porous media usually evaluate microbial reactions with Monod kinetics and rate constants measured on well-mixed laboratory cultures, in which every cell is exposed to the same substrate concentration. In natural sediments and aquifers this assumption fails at the pore scale, because the cells are not suspended but reside in biofilms and aggregates attached to the grains, into which the limiting substrate must diffuse while the cells consume it. The interior of a biofilm is therefore starved relative to its surface, and the rate that a continuum model should assign to the average pore-water concentration falls below the laboratory Monod rate. Here we ask how large this reduction is, what controls it, and whether it can be captured in a single correction that a continuum model can apply. We reduce the steady reaction-diffusion problem inside the film to dimensionless form, which leaves one controlling group, a Thiele modulus equal to the square root of a Damkohler number that measures how strongly diffusion limits the reaction. Integrating the governing equation once gives the reduction explicitly, as a biofilm effectiveness factor: it equals the classical hyperbolic-tangent law when the surface is dilute and a half-power, partial-penetration law when it is saturated, and the uptake of a thick biofilm follows a law whose apparent reaction order slides continuously from one to one-half. A direct consequence is that the half-saturation constant fitted to such a community exceeds its true value, and we quantify the excess: the apparent constant is 1.2 times the intrinsic one at a Thiele modulus of one, 15 times at ten, and approaches one eighth of the Damkohler number when diffusion dominates. Multiplied by the biofilm surface area per unit volume, the effectiveness factor becomes a drop-in rate correction for continuum reactive-transport models, accurate to better than a percent provided the substrate is drawn down by less than about a fifth across a grid cell, and provided the external boundary layer is not itself limiting. Applied to the anaerobic oxidation of methane in marine sediments, the same formulas act as a screening test, and on current estimates of aggregate size and rate they indicate that such aggregates are reaction-limited and that their measured kinetics are close to intrinsic.

Article Highlights

- An explicit biofilm effectiveness factor, governed by a Thiele modulus equal to the square root of the Damköhler number, corrects intrinsic Monod rates for diffusion limitation within biofilms at the pore scale.

- Within a thick biofilm the uptake flux shifts the apparent reaction order from first to half order and raises the half-saturation constant fitted to a community above its intrinsic value, by a factor of 1.2 at a Thiele modulus of one and 15 at ten, approaching one eighth of the Damkohler number.

- Multiplied by the biofilm surface area, the factor becomes a drop-in upscaling correction for continuum reactive-transport codes, with stated conditions of validity; applied as a screening test to methane-oxidising aggregates it indicates intrinsic rather than transport-limited kinetics.

Keywords Reactive transport, Biofilm, Effectiveness factor, Monod kinetics, Thiele modulus, Upscaling

1. Introduction

Microbial reactions drive much of the chemistry of the subsurface, including denitrification, sulfate reduction, iron and manganese cycling, contaminant degradation, and the anaerobic oxidation of methane, and a microbial rate law lies at the centre of every reactive-transport model of these processes (Monod 1949; Dentz et al. 2011). That rate law is almost always written in the form Monod proposed, in which a maximum rate is multiplied by a saturating dependence on the substrate concentration. Its parameters are measured on suspended, well-mixed cultures, in which every cell is exposed to the same concentration. In a porous medium this assumption fails at the pore scale (Blunt et al. 2013). The microbes are not suspended but reside in biofilms that coat the grain surfaces and in dense aggregates lodged in the pore space (Wood and Whitaker 1998), and the substrate must diffuse into these structures against the gradient the cells create as they consume it. The interior of a biofilm is therefore depleted relative to its surface, the cells there react below their intrinsic rate, and the rate that a continuum (Darcy-scale) model assigns to the bulk concentration is a transport-limited effective rate rather than the intrinsic Monod rate.

This is the microbial version of a problem long studied in catalysis and reactor engineering, in which a reaction is limited by the rate at which transport supplies it rather than by the chemistry itself. Thiele (1939) showed that a porous catalyst grain large enough to be diffusion-limited reacts only in a thin layer near its surface, and quantified the loss with an effectiveness factor, the ratio of the rate actually achieved to the rate the grain would reach if its entire interior were exposed to the surface concentration (Aris 1975). The same construction was later carried into biofilm modeling, where it accounts for the dependence of measured rates on biofilm thickness and substrate concentration, and for the shift from apparently first-order to half-order kinetics in thick films (Williamson and McCarty 1976; Harremoës 1978; Rittmann and McCarty 1980). Subsequent work that volume-averaged diffusion and reaction in biofilms (Wood and Whitaker 1998) and treated the macrotransport of biologically reacting solutes (Dykaar and Kitanidis 1996) placed these ideas on the continuum footing that reactive-transport models require, in effect upscaling a pore-scale diffusion-reaction process to an effective Darcy-scale rate.

What these literatures lack is a single, compact statement of the result in the language that a pore-scale reactive-transport modeler already uses. The effectiveness factor, the half-order biofilm limit, and the volume-averaged rate are usually presented separately, in catalysis or wastewater-engineering notation, and are rarely connected to the Damkohler number, the effective rate, and the upscaling framework through which the porous-media community reads mixing-limited reactions (Battiato and Tartakovsky 2011; Dentz et al. 2011). The consequence that matters most to a modeler, that the Monod parameters fitted to a biofilm community describe transport as much as enzyme kinetics, is itself long established in the immobilized-enzyme and catalysis literature, where diffusion is known to raise the apparent Michaelis constant of an immobilized preparation above its intrinsic value (Engasser and Horvath 1973; Goldstein 1976). What is missing is not that result but its translation, and it is easily overlooked when laboratory rates are placed in a continuum code.

In the present study we compute that reduction directly. The community is represented as a continuum rather than cell by cell, a homogeneous layer of biomass of fixed thickness on the grain surface, in which every cell obeys the Monod rate law measured in the laboratory on suspended cells. No water flows inside that layer, so substrate can only diffuse in, and what the model resolves is the substrate concentration at each depth. That concentration falls as it goes, because every cell the substrate passes consumes some of it, leaving the cells nearest the grain hungry. The calculation needs four numbers a modeler already has, the thickness of the layer, the effective diffusivity inside it, the maximum rate the cells can sustain, and the half-saturation constant, and these combine into one number, the Thiele modulus, which asks whether substrate crosses the layer faster than the cells can eat it. We solve the steady balance between diffusion and consumption twice, once by integrating the governing equation by hand and once with an independent finite-difference solver. Dividing the substrate that enters the layer by the amount those cells would consume if all of them saw the outer concentration gives the effectiveness factor, the fraction of the laboratory rate the community realizes, which multiplied by the biofilm area per unit volume becomes a rate a continuum code can use in place of Monod kinetics at the grid-average concentration. We then test what that step assumes, by adding a resisting boundary layer outside the film, by repeating the solve for a sphere instead of a flat layer, and by checking the volumetric rate against a resolved chain of pores. On that basis we answer three questions. How far below the laboratory rate does diffusion push the realized rate, and what sets the size of the gap? By how much are the Monod parameters fitted to such a community distorted, in particular the half-saturation constant? And under what conditions may the correction be used in a continuum model, and when does it fail? Section 2 sets out the biofilm problem, the analytical solution and the numerical procedure, Section 3 reports the results, and Sections 4 and 5 discuss and conclude.

2. Methods

2.1. The biofilm reaction-diffusion problem

We represent a biofilm as a thin planar layer of biomass of thickness L_f attached to a grain surface and bathed by pore water that holds the limiting substrate at concentration S_b at the biofilm surface. Within the film the substrate diffuses with an effective diffusivity D_e and is consumed by the resident cells following Monod kinetics, so the volumetric uptake rate is

$$R(S) = r_{max}\,\frac{S}{K_s+S}, \qquad r_{max} = q_{max}X, \tag{1}$$

where R(S) is the volumetric uptake rate of the biofilm, S the local substrate concentration, r_max the maximum volumetric rate, q_max the maximum specific uptake rate, X the biomass density and K_s the intrinsic half-saturation constant.

where q_{max} is the maximum specific uptake rate, X the biomass density, and K_s the half-saturation constant. At steady state the substrate that diffuses into the film is balanced by the substrate consumed within it, so that diffusion balances reaction:

$$D_e\,\frac{\mathrm{d}^2S}{\mathrm{d}z^2} = R(S), \qquad S(0) = S_b, \quad \left.\frac{\mathrm{dS}}{\mathrm{dz}}\right|_{z=L_f} = 0, \tag{2}$$

where D_e is the effective diffusivity of the substrate inside the film, z the depth measured inward from the outer surface, S_b the substrate concentration in the pore water at that surface, and L_f the film thickness, so that the second condition states that no substrate crosses into the grain.

Here z is measured inward from the outer surface, and the no-flux condition at the grain wall, where $z = L_f$, expresses that no substrate crosses into the grain. Scaling concentration by the half-saturation constant and depth by the film thickness, through $s = S/K_s$, $\beta = S_b/K_s$, and $\zeta = z/L_f$, reduces the governing equation to a single dimensionless parameter,

$$\frac{\mathrm{d}^2s}{\mathrm{d}\zeta^2} = \phi^2\,\frac{s}{1+s}, \qquad s(0) = \beta, \quad \left.\frac{\mathrm{ds}}{\mathrm{d}\zeta}\right|_{\zeta=1} = 0, \tag{3}$$

where s = S/K_s is the concentration scaled by the half-saturation constant, zeta = z/L_f the depth scaled by the film thickness, beta = S_b/K_s the surface saturation, and phi the Thiele modulus defined next.

in which that parameter is the Thiele modulus, a measure of how strongly diffusion limits the reaction,

$$\phi = L_f\sqrt{\frac{r_{max}}{K_sD_e}} = \sqrt{\mathrm{Da}}, \qquad Da = \frac{L_f^2\,r_{max}}{K_sD_e}. \tag{4}$$

where phi is the Thiele modulus, Da the Damkohler number, L_f the film thickness, r_max the maximum volumetric rate, K_s the half-saturation constant and D_e the effective diffusivity, so that phi is the square root of Da.

The Thiele modulus has a direct physical interpretation. The underlying Damköhler number compares the time for substrate to diffuse across the film with the time for the cells to consume it, and the Thiele modulus is its square root. Two regimes follow. When the Thiele modulus is small, diffusion is rapid relative to reaction and the film is supplied uniformly. When it is large, reaction outpaces diffusion and the interior of the film is starved. The scaled surface concentration sets where on the Monod curve the surface lies, from first-order behavior at low saturation to saturated, zero-order behavior at high saturation.

Two qualifications belong with this definition. First, the modulus in Equation (4) is built from the low-concentration slope of the Monod law, r_max/K_s, so it is the first-order modulus. It is used in that form consistently throughout the paper and in every figure, but it is not the natural scaling for a saturated film, for which the generalized modulus of Appendix A.12 absorbs the saturation dependence and is the appropriate variable.

Second, the surface condition S(0) = S_b assumes that the concentration at the biofilm surface equals the bulk pore-water concentration, that is, that the diffusive boundary layer outside the film offers no resistance. The resistance of that layer is measured by a Biot number Bi = k_L L_f / D_e, in which k_L is the external mass-transfer coefficient, and the assumption is exact only in the limit of large Bi. To quantify the error it introduces we also solved the same problem with the Robin condition that the external flux k_L(S_b - S(0)) equals the flux entering the film, and Section 3.3 reports the result.

The analysis above is for a planar film, whereas aggregates are closer to spheres. To measure how far the two geometries differ we also solved the spherical problem, in which the radius R replaces the film thickness and the Laplacian carries the extra curvature term, and compared it with the slab both at the same modulus and after normalizing by the shape length, the ratio of volume to external surface, which is L_f for a slab and R/3 for a sphere. Section 3.2 reports the comparison.

Table 1. Notation. Dimensionless groups are marked with a dash in the units column. The scalings s = S/K_s, beta = S_b/K_s and zeta = z/L_f are used throughout, with the surface at zeta = 0 and the grain wall at zeta = 1.

Symbol	Meaning	Units
S	local substrate concentration inside the film	mol m-3
S_b	substrate concentration in the pore water at the film surface	mol m-3
s, beta	S/K_s and S_b/K_s, dimensionless concentration and surface saturation	-
s_w	dimensionless concentration at the grain wall	-

z, zeta	depth measured inward from the surface, and z/L_f	m, -
L_f	biofilm thickness	m
D_e	effective diffusivity of the substrate inside the film	m2 s-1
q_max	maximum specific uptake rate	mol kg-1 s-1
X	biomass density	kg m-3
r_max	maximum volumetric rate, q_max X	mol m-3 s-1
K_s	intrinsic half-saturation constant	mol m-3
R(S)	local volumetric uptake rate	mol m-3 s-1
phi	Thiele modulus, L_f sqrt(r_max/(K_s D_e))	-
Da	Damkohler number, equal to phi squared	-
eta	effectiveness factor	-
G(s)	first-integral potential, s - ln(1+s)	-
J	substrate flux into the film per unit surface area	mol m-2 s-1
a_v	biofilm surface area per unit volume of porous medium	m-1
n_app	apparent reaction order	-
Phi_g	generalized (Bischoff) modulus	-
k_L	external mass-transfer coefficient of the boundary layer	m s-1
Bi	Biot number for external transfer, k_L L_f / D_e	-
R, Lambda	aggregate radius, and shape length equal to volume over external surface	m

2.2. The effectiveness factor

The quantity a continuum model requires is the effectiveness factor η, the fraction of the intrinsic rate that the film actually realizes. We define it as the uptake of the whole film divided by the uptake it would realize if every cell were exposed to the surface concentration:

$$\eta = \frac{\int_0^1 \frac{s}{1+s} d\zeta}{\frac{\beta}{1+\beta}} \in (0,1]. \quad (5)$$

where eta is the effectiveness factor, the integral in the numerator is the uptake the film actually realizes, and the denominator beta/(1+beta) is the uptake it would realize if every cell were exposed to the surface concentration.

Integrating the governing equation once makes the effectiveness factor explicit. Multiplying the equation by the concentration gradient casts it as an exact derivative, which is integrated inward from the grain wall, where the concentration equals its wall value and the gradient vanishes, to give

$$\left(\frac{\mathrm{ds}}{\mathrm{d}\zeta}\right)^2 = 2\phi^2[\,G(s) - G(s_w)\,], \qquad G(s) = s - ln(1+s), \tag{6}$$

where G(s) = s - ln(1+s) is the potential whose derivative is the local dimensionless uptake s/(1+s), s_w is the concentration at the grain wall, and the left-hand side is the square of the dimensionless concentration gradient.

so that the dimensionless flux of substrate entering the film at the surface is fixed by the surface and wall concentrations. Because this surface flux equals the total uptake of the film, the effectiveness factor follows directly,

$$\eta = \frac{\sqrt{2\,[\,G(\beta) - G(s_w)\,]}}{\phi} \cdot \frac{1+\beta}{\beta}, \tag{7}$$

where eta is again the effectiveness factor, beta the surface saturation, phi the Thiele modulus and s_w the wall concentration, which is the only quantity not yet known.

where the only remaining unknown, the concentration at the grain wall, is determined by the film thickness through

$$\int_{s_w}^{\beta} \frac{\mathrm{ds}}{\sqrt{2[\,G(s) - G(s_w)\,]}} = \phi. \tag{8}$$

where the integral runs from the wall concentration s_w up to the surface saturation beta, and setting it equal to the Thiele modulus phi expresses that the film has unit dimensionless thickness, which fixes s_w.

2.3. Limiting laws

Two limiting cases admit explicit expressions and bracket the behavior.

First-order limit (dilute surface). When the surface concentration is well below the half-saturation constant, the kinetics become linear in concentration, and the substrate profile through the film is a hyperbolic cosine centred on the grain wall. The effectiveness factor then reduces to the classical Thiele result for a flat layer (Thiele 1939; Aris 1975),

$$\eta = \frac{tanh\phi}{\phi}, \tag{9}$$

where phi is the Thiele modulus, so that this is the classical hyperbolic-tangent result for a flat layer under first-order kinetics.

which approaches one when the Thiele modulus is small and falls in inverse proportion to the Thiele modulus when it is large. This is the grey reference curve in Figure 1.

Zero-order limit with partial penetration (saturated surface). When the surface is saturated, the cells consume at a constant rate as long as substrate remains, so the substrate is exhausted at a finite penetration depth, which measures how far it reaches into the film before it is consumed. If that depth exceeds the film thickness the film is fully penetrated and the effectiveness factor is one; if it is smaller, only the outer fraction of the film is active, and

$$\eta \simeq \frac{\sqrt{2\beta}}{\phi}, \tag{10}$$

where beta is the surface saturation and phi the Thiele modulus, and the expression holds once phi exceeds the square root of 2 beta, the point at which the substrate no longer reaches the wall.

a half-power dependence on the surface saturation that signals incomplete penetration. The full Monod solution of Section 2.2 passes continuously between these two limits.

2.4. Deep-biofilm flux and apparent reaction order

When the film is thick compared with the penetration depth, as is common for active aggregates, the wall concentration vanishes and the flux into the film becomes independent of thickness. Setting the wall concentration to zero in the integrated equation gives an explicit deep-biofilm uptake flux,

$$J = \sqrt{2D_e\, r_{max}\, [\, S_b - K_s ln(1 + S_b/K_s)\,]}, \tag{11}$$

where J is the substrate flux entering the film per unit surface area, D_e the effective diffusivity, r_max the maximum volumetric rate, S_b the bulk substrate concentration and K_s the half-saturation constant, the flux being independent of film thickness in this limit.

which is the dimensional form of the result of Harremoës and of Rittmann and McCarty (Harremoës 1978; Rittmann and McCarty 1980). Its meaning is clearest in the apparent reaction order, the order one would infer by fitting measured rate against substrate concentration, defined as the slope of the logarithm of the flux against the logarithm of the bulk concentration,

$$n_{app} = \frac{\mathrm{dln J}}{\mathrm{dln} S_b} = \frac{1}{2}\,\frac{S_b}{S_b + K_s} \cdot \frac{S_b}{S_b - K_s ln(1 + S_b/K_s)}. \tag{12}$$

where n_app is the apparent reaction order that would be inferred by fitting measured rate against substrate concentration, S_b the bulk concentration and K_s the half-saturation constant.

2.5. Upscaling to the pore network

For a continuum reactive-transport model the relevant quantity is the uptake per unit volume of porous medium. If the biofilm presents a surface area a_v per unit volume of medium to the pore water, the macroscopic uptake rate in the deep-film regime is the surface flux multiplied by that area,

$$\mathcal{R}_{macro}(S_b) = a_v J(S_b) = a_v\sqrt{2D_e\, r_{max}[\, S_b - K_s ln(1 + S_b/K_s)\,]}, \qquad (13)$$

where R_macro is the uptake per unit volume of porous medium, a_v the biofilm surface area per unit volume, and J the surface flux of Equation (11).

and more generally the macroscopic rate is the effectiveness factor times the biofilm volume fraction times the intrinsic Monod rate evaluated at the bulk concentration, in which the effectiveness factor of Section 2.2 supplies the correction to the naive product of biomass and intrinsic rate. Equation (13) is a closure rather than a derived result, and it rests on four assumptions that should be stated plainly. (i) Every biofilm in the averaging volume sees the same substrate concentration, the volume-averaged pore-water value, so that no gradient between biofilms is resolved. (ii) The biofilms are independent, so that one does not deplete the supply of another. (iii) The effectiveness factor computed for a single film applies pore by pore. (iv) The area density a_v and the film thickness L_f are uniform within the averaging volume. A formal derivation would obtain Equation (13) by volume averaging with an explicit closure for the deviation concentration, in the manner of the volume-averaged biofilm equations (Wood and Whitaker 1998) and the macrotransport theory of biologically reacting solutes (Dykaar and Kitanidis 1996). We do not carry out that derivation here.

2.6. Numerical solution

Because the effectiveness factor is obtained by integrating the governing equation once, it is worth verifying both that step and its limiting laws against a fully independent numerical solution. We solved the steady reaction-diffusion equation with its two boundary conditions, the prescribed surface concentration and the no-flux condition at the grain wall, with a standard finite-difference scheme on a discretized biofilm, computed the effectiveness factor from the resulting profile, and compared it with the explicit formula and with the limits of Section 2.3.

3. Results

3.1. The effectiveness factor and the substrate profiles

Equations (6) to (8) constitute the complete solution: for a given Thiele modulus and surface saturation, the thickness condition determines the wall concentration, which in turn determines the effectiveness factor. Figure 1 shows the result. When the Thiele

modulus is small the film is fully supplied, the wall concentration approaches the surface value, the effectiveness factor approaches one, and the intrinsic Monod rate is recovered. When the Thiele modulus is large the interior is exhausted, the wall concentration falls to zero, the effectiveness factor falls in inverse proportion to the Thiele modulus, and the realized rate is set by how fast substrate diffuses into the film rather than by the kinetics. The surface saturation controls the transition: a saturated film remains fully effective to larger Thiele moduli, because zero-order kinetics allow the substrate to penetrate further before it is exhausted.

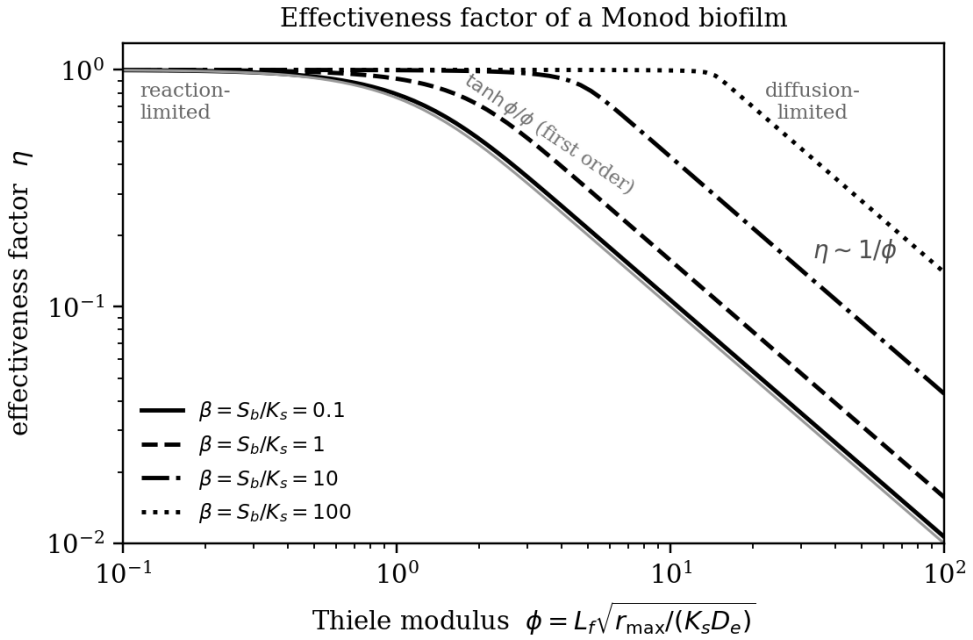

Figure 1. Effectiveness factor η of a Monod biofilm as a function of the Thiele modulus ϕ, for surface saturations $\beta = S_b/K_s = 0.1,1,10,100$. At low Thiele modulus the film is reaction-limited and the effectiveness factor approaches one, recovering the intrinsic kinetics; at high Thiele modulus it is diffusion-limited and the factor falls in inverse proportion to the modulus. The grey line is the first-order limit $\eta = tanh\phi/\phi$, which the lowest-saturation curve follows; higher saturation keeps the film fully effective to larger Thiele moduli.

The substrate profiles underlying these effectiveness factors are shown in Figure 2 for a saturated film. As the Thiele modulus increases, the substrate is drawn down increasingly steeply from the surface, and beyond a threshold it falls to zero at a finite depth, leaving the deep biomass inactive. It is this inactive interior that the effectiveness factor measures.

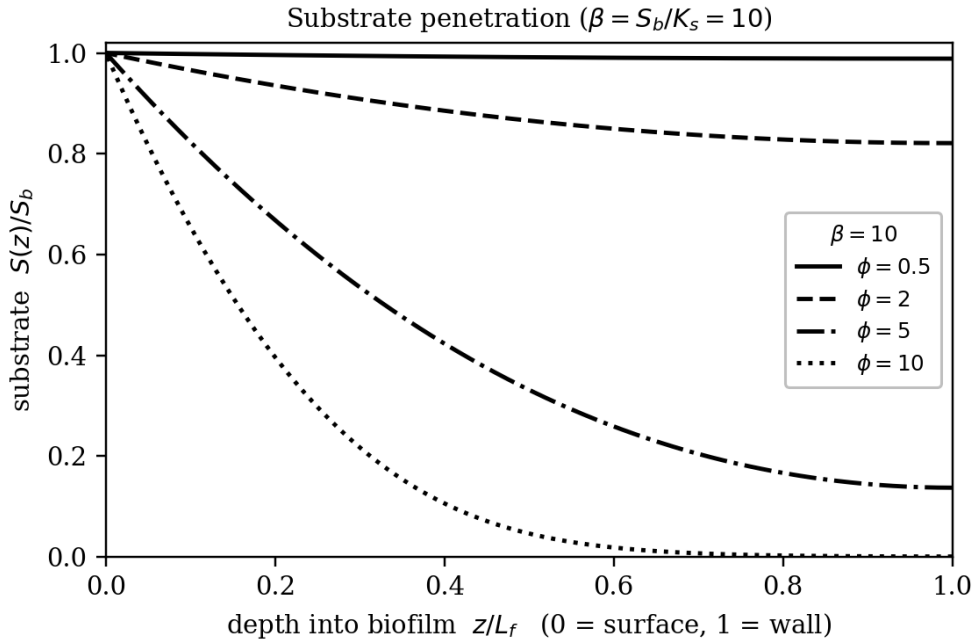

Figure 2. Steady substrate profiles inside the biofilm, the local concentration s against dimensionless depth (surface on the left, grain wall on the right), for a saturated film at Thiele moduli 0.5, 2, 5 and 10. The profiles are obtained by shooting on the first integral, integrating Equation (6) inward from the wall concentration fixed by Equation (8). At low Thiele modulus the film is nearly uniform; at high Thiele modulus the substrate is confined to a thin surface layer and is exhausted before the wall, leaving the deep biomass starved.$S(z)/S_b z/L_f \phi =$ 0.5,2,5,10

3.2. Planar film against spherical aggregate

One geometric caveat applies to everything above. The analysis is for a planar film, whereas aggregates are closer to spheres, and the two geometries do not give the same effectiveness factor at the same modulus. Solving the spherical problem, with the radius R in place of the film thickness, gives a factor well above the slab value, 0.51 against 0.21 at a modulus of 5 and a dilute surface, because a sphere presents more surface per unit volume. The classical remedy is to normalize by the shape length, the ratio of volume to external surface, which is L_f for a slab and R/3 for a sphere. Doing so collapses the two geometries to within about 20 % across moduli from 0.5 to 20 and surface saturations from 0.1 to 10. The worst departure, 16 % in our solve, occurs at the largest modulus and the most saturated surface tested, a modulus of 20 at a saturation of 10, and an independently written solver puts it at 19 %. The shape-normalized slab formula is therefore adequate for screening, while quantitative work on aggregates should use the spherical solution, which the deposited code provides.

3.3. Effect of the external boundary layer

Replacing the fixed surface concentration by the Robin condition of Section 2.1 shows how much the neglect of the external boundary layer costs. At Bi = 10 it overestimates the effectiveness factor by 0.6 % at a Thiele modulus of 0.5, by 9.8 % at 2, by 25.1 % at 5 and by 59.0 % at 20, and at Bi = 100 the same errors fall to 0.1 %, 1.0 %, 3.1 % and 11.5 %, all computed at beta = 1, where the pore-water concentration equals the half-saturation constant. The error therefore grows with the Thiele modulus, and the internal-resistance-only treatment is accurate to a few percent provided Bi exceeds roughly ten times the Thiele modulus. In the slow flows of fine-grained sediments that condition is not automatic, and where it fails the two resistances must be combined in series.

3.4. Apparent reaction order and apparent half-saturation constant

Two limits bracket Equation (12). When the surface concentration is well below the half-saturation constant, the uptake flux is proportional to the concentration and the apparent order is one, that is, first-order kinetics. When it is well above, the flux is proportional to the square root of the concentration and the apparent order is one-half, that is, half-order kinetics. A transport-limited biofilm therefore exhibits an apparent reaction order that changes continuously from one to one-half as the substrate concentration increases (Figure 3).

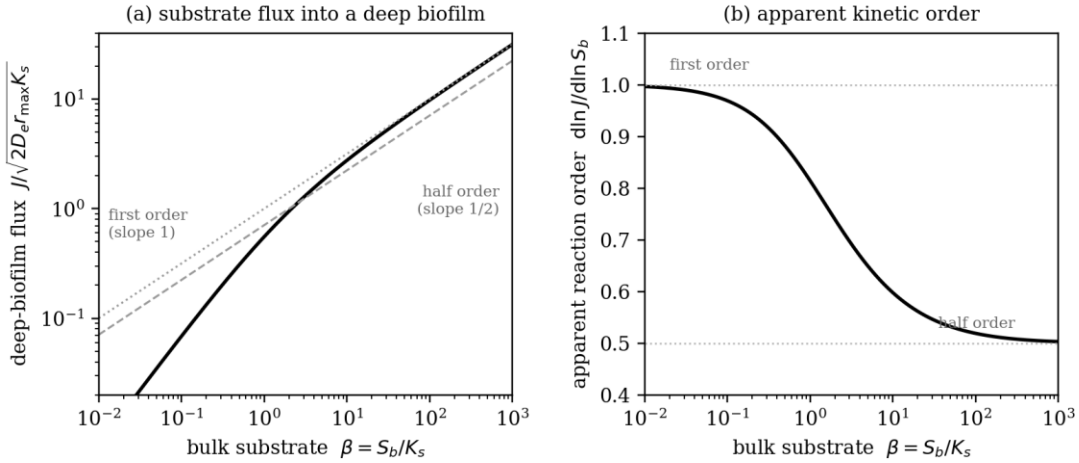

Figure 3. Deep-biofilm kinetics from the explicit uptake flux. (a) Dimensionless substrate uptake flux against bulk concentration, with the first-order limit (slope one) and the half-order limit (slope one-half). (b) Apparent reaction order, running continuously from one at low concentration to one-half at high concentration.

This continuous change in apparent order has a practical consequence that is easily overlooked. If the bulk uptake flux of a transport-limited community is fitted to a Monod form, the half-saturation constant obtained is not the intrinsic value of the organisms but an apparent value raised by diffusion limitation. Because the interior of the film is starved,

the community reaches half of its maximum flux only at a bulk concentration above the intrinsic half-saturation constant. This is the biofilm form of an effect established for immobilized enzymes and porous catalysts, in which the apparent Michaelis constant of a diffusion-limited preparation exceeds the intrinsic one and grows with the size of the support (Engasser and Horvath 1973; Goldstein 1976). Reported half-saturation constants for biofilms and aggregates are therefore in part descriptions of transport rather than of enzyme kinetics, and they should be expected to increase with aggregate size and to depend on flow, just as effective rates in abiotic systems depend on scale and velocity (Battiato and Tartakovsky 2011).

The size of that shift can be computed, and it is large. A finite film is needed to define it, because the deep-film flux of Equation (11) grows without bound and has no half-maximum. For a film of thickness L_f the uptake per unit surface area is the effectiveness factor times the intrinsic rate times the thickness, and it saturates at r_max L_f as the surface becomes zero order, so the apparent half-saturation constant is the bulk concentration at which the uptake reaches half of that value. In dimensionless form K_app/K_s is the saturation beta solving eta(phi, beta) beta/(1+beta) = 1/2. Table 2 gives the result. The apparent constant equals the intrinsic one when diffusion is fast, exceeds it by 17 % at a Thiele modulus of one, by a factor of 2.5 at three, 15 at ten, 117 at thirty and 1257 at one hundred. In the diffusion-limited limit the condition reduces to G(beta) = phi^2/8, and since G(beta) tends to beta for large beta the artifact has the compact asymptote

$$K_{app} / K_s \to \phi^2 / 8 = Da / 8 ,$$

which the numerical values approach to within 4 % at a Thiele modulus of thirty and 0.6 % at one hundred. Two cautions attach to this number. It depends on the Thiele modulus and is therefore meaningless unless the modulus is quoted with it, and it depends on the range of concentrations over which the Monod form is fitted, since a fit confined to low concentrations recovers a value closer to the intrinsic one. Quoted half-saturation constants for biofilms and aggregates should therefore carry the size of the structure and the concentration range of the fit.

Table 2. Apparent half-saturation constant of a finite Monod film, defined as the bulk concentration at which the uptake reaches half of its saturation value r_max L_f. The last two columns show the diffusion-limited asymptote Da/8 and its ratio to the computed value. Computed by REVISION_computations.py and deposited in apparent_half_saturation.csv.

Thiele modulus phi	Damkohler number Da	K_app / K_s	Asymptote Da/8	Ratio to asymptote
0.1	0.01	1.002	0.00125	801
0.3	0.09	1.015	0.011	90.2
1	1	1.167	0.125	9.33
3	9	2.475	1.125	2.20
10	100	15.29	12.50	1.22

30	900	117.3	112.5	1.04
100	10000	1257	1250	1.01

3.5. Accuracy of the upscaled rate

Assumption (i) is the one most easily violated, and it can be tested directly. We modeled a representative elementary volume as a chain of well-mixed pores in series, each losing substrate to its own biofilm at the deep-film flux of Equation (11), and compared the resolved uptake, which is the average of the flux over the pores, with the closure, which is the flux evaluated at the average concentration. Because the flux is concave in concentration the closure overestimates. The overestimate is 0.06 % or less while no more than 20 % of the substrate is consumed across the averaging volume, rises to about 1 % at 60 % consumption and to 2.9 % at 80 %, and the insensitivity to inlet saturation holds only while the drawdown is small: at 80 % consumption the error ranges from 0.8 % at an inlet saturation of 0.3 to 2.9 % at 30. Equation (13) is therefore accurate to well under a percent provided the grid cell is small enough that the substrate is drawn down by less than about a fifth across it, which is the condition a modeler should check. The test does not probe assumptions (ii) to (iv), which remain untested here.

3.6. Verification against independent numerical solutions

The agreement is complete (Figure 4). On the grid used for the figure the finite-difference and explicit effectiveness factors differ by at most 1.2 x 10^-6 across three orders of magnitude in the Thiele modulus and over four decades of surface saturation. The difference falls as the square of the grid spacing, from 1.2 x 10^-4 on 300 intervals to 1.1 x 10^-5 on 1000, 1.2 x 10^-6 on 3000 and 1.1 x 10^-7 on 10 000, the worst case in every case being the thin surface layer at a Thiele modulus of 100 and a dilute surface. This confirms that the explicit expression is exact and that both numerical routes are reliable. The first-order and partial-penetration limits track the low- and high-saturation curves respectively in the diffusion-limited regime, each within its range of validity. The expressions presented as the working results of this study are therefore faithful to the full reaction-diffusion problem and not merely to its limiting behavior.

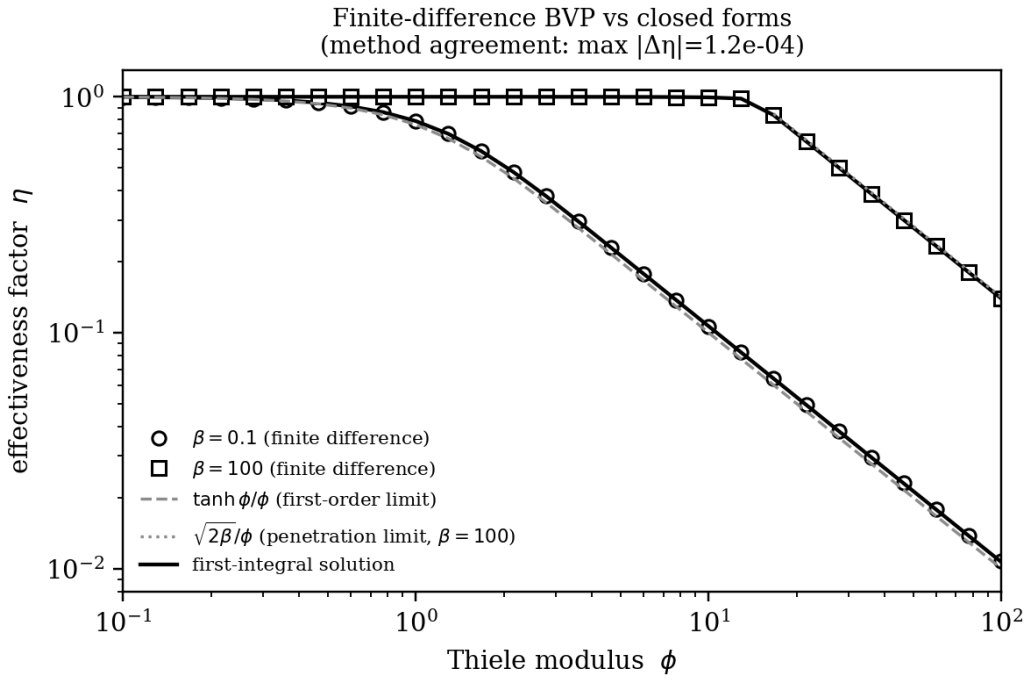

Figure 4. Validation of the effectiveness factor against an independent finite-difference solution of the biofilm equation. The markers are the finite-difference solution at low and high surface saturation, the solid lines are the explicit formula, and on the grid used here the two differ by at most 1.2 x 10^-6. The grey curves are the explicit limits, the first-order law (dashed) and the partial-penetration law (dotted), each tracking its regime.

An internal asymptotic consistency check. The comparison above tests the explicit formula against an independent numerical solution of the same problem. A second check asks whether the formula behaves as the generalized-modulus construction requires. Bischoff (1965) showed that the effectiveness factor of a flat layer collapses onto a single curve when it is plotted against a modulus that weights the rate by its own integral, along which the product of the effectiveness factor and the generalized modulus tends to one in the diffusion-limited regime. Figure 5 plots the explicit effectiveness factor in both variables. Against the ordinary Thiele modulus the curves for surface saturations spanning four decades spread across the diagram (panel a); against the generalized modulus they collapse onto the universal curve (panel b), and the residual departure from unity is 2.8 x 10^-5 once the modulus is moderately large. We state plainly what this does and does not establish. Substituting the deep-film limit of Equation (7) into the generalized modulus of Appendix A.12 gives a product identically equal to one, which we confirm to ten digits, so the collapse is an algebraic identity rather than independent evidence, no data from Bischoff (1965) are used, and only Monod kinetics are tested. The residual 2.8 x 10^-5 measures the departure of the finite-thickness solution from that limit, and the check is presented in that spirit, as confirmation that the quadrature and the root find are converged.

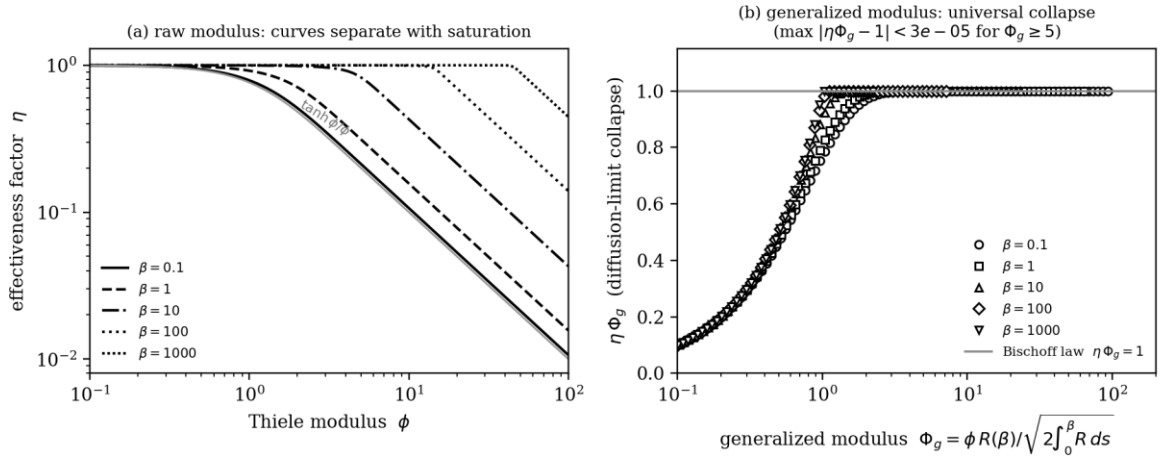

Figure 5. Internal consistency of the explicit effectiveness factor with the generalized-modulus construction of Bischoff (1965). (a) The explicit effectiveness factor against the ordinary Thiele modulus, for surface saturations spanning four decades; the curves separate because the Thiele modulus alone does not absorb the saturation dependence. (b) The same effectiveness factors against the generalized modulus collapse onto a single curve along which the product of the effectiveness factor and the generalized modulus equals one. The collapse is an algebraic identity in the deep-film limit rather than an external benchmark, and the residual departure of 2.8 x 10^-5 measures the finite thickness of the film.

4. Discussion

The theory presented here is a synthesis. The effectiveness factor descends from Thiele (1939) and Aris (1975), the biofilm half-order limit from Harremoës (1978) and from Williamson and McCarty (1976) and Rittmann and McCarty (1980), and the continuum formulation from Wood and Whitaker (1998) and from Dykaar and Kitanidis (1996). Its contribution is to collect these results into explicit expressions written in a single Thiele and Damköhler variable, and to make explicit the consequence that matters most to a modeler: in a porous medium the apparent Monod parameters are modified by transport, with the half-saturation constant inflated and the apparent order pushed toward one-half wherever diffusion limits the supply of substrate. The resulting procedure is simple. From estimates of the biofilm or aggregate thickness, the effective diffusivity, the maximum rate, and the half-saturation constant, one forms the Thiele modulus. If it exceeds about one, the intrinsic Monod rate overestimates the realized rate by the inverse of the effectiveness factor, and the effectiveness-factor or deep-film expression should be used in its place.

The structure of the closure mirrors the abiotic case. There, incomplete mixing of two reactants lowers a bimolecular rate (de Anna et al. 2014), whereas here, incomplete diffusion of a single substrate into a biofilm lowers a Monod rate. In both cases a single dimensionless group, a Damkohler number comparing reaction to transport, determines whether the rate a model uses represents the intrinsic chemistry or a disguised transport

rate (Battiato and Tartakovsky 2011). Where the bulk flow is slow, the external resistance quantified in Section 3.3 must be placed in series with the internal one.

The most direct application of this framework is to the aggregate-hosted reactions of marine sediments, and in particular to the anaerobic oxidation of methane, in which consortia of archaea and bacteria form dense aggregates a few tens of micrometres across, into which methane and sulfate must diffuse (Boetius et al. 2000). Such aggregates are natural diffusion-reaction structures, and it is worth carrying out the estimate the theory prescribes rather than asserting that transport matters. Table 3 collects the quantities needed and shows the arithmetic, so that a reader can substitute their own values. Taking the effective diffusivity of methane inside an aggregate as half its free-solution value at 4 degrees Celsius, 5 x 10^-10 m2 s-1, and building the maximum volumetric rate from a cell-specific rate of 1 fmol per cell per day at a cell density of 10^17 cells m-3, which gives 1.2 x 10^-3 mol m-3 s-1, the radius at which the Thiele modulus reaches one is R* = sqrt(K_s D_e / r_max) and lies between about 66 and 660 micrometres for half-saturation constants between 0.01 and 1 mol m-3. Observed aggregate radii of 5 to 50 micrometres are therefore an order of magnitude smaller than R*, the Thiele modulus is 0.03 to 0.3, and the spherical effectiveness factor exceeds 0.998.

The conclusion of that estimate is worth stating plainly, because it qualifies the application. On these numbers a methane-limited AOM aggregate is reaction-limited, not diffusion-limited, and its measured kinetics are close to intrinsic. The correction derived here becomes material only if the volumetric rate is about two orders of magnitude larger than the central estimate, if the aggregate is several hundred micrometres across, or if the limiting substrate has a much smaller half-saturation constant or diffusivity than methane. At a rate a hundred times the central value the Thiele modulus of a 20 micrometre aggregate reaches 0.96 and the effectiveness factor falls to 0.985, which is still a small correction. Since published estimates of cell-specific AOM rates and of aggregate half-saturation constants span more than an order of magnitude (Nauhaus et al. 2007; Orcutt and Meile 2008; Dale et al. 2008), the screening calculation of Table 3 is the appropriate way to decide the question for a particular site, and on present numbers it decides it in favour of intrinsic kinetics.

Table 3. Worked estimate of the Thiele modulus for an anaerobic methane-oxidising consortium aggregate. Every input is an order of magnitude with its basis stated, and the arithmetic is shown so that a reader may substitute site-specific values. On these numbers the aggregates are reaction-limited, and the diffusion correction is negligible.

Quantity	Value used	Basis
Aggregate radius R	5 to 50 um	observed consortium size (Boetius et al. 2000)
Free-solution diffusivity of CH4 at 4 C	1.0 x 10-9 m2 s-1	standard value for seawater
Effective diffusivity D_e inside the aggregate	5 x 10-10 m2 s-1	half the free-solution value
Cell-specific AOM rate	1 fmol cell-1 d-1	order of magnitude from in vitro rates (Nauhaus et al. 2007)

Cell density inside the aggregate	1 x 10^17 cells m-3	close packing of micrometre cells
Maximum volumetric rate r_max	1.2 x 10-3 mol m-3 s-1	product of the two lines above
Half-saturation constant K_s for CH4	0.01 to 1 mol m-3	range spanned by published estimates
Critical radius R* at which phi_R = 1	66 to 660 um	sqrt(K_s D_e / r_max)
Thiele modulus phi_R at R = 20 um	0.03 to 0.3	R sqrt(r_max/(K_s D_e))
Spherical effectiveness factor at beta = 1	greater than 0.998	spherical solution of Section 4

The limitations of the analysis point directly to its extensions. The model assumes a single limiting substrate, whereas the anaerobic oxidation of methane and many other sediment processes are governed by two co-diffusing substrates and by syntrophic coupling, which would replace the single Thiele modulus with a pair and introduce counter-diffusion. The biofilm is treated as a homogeneous flat layer of fixed thickness, whereas real aggregates are curved and heterogeneous and grow in response to the very gradients computed here, which couples the effectiveness factor to a moving-boundary problem. Finally, the substrate is treated as conservative outside the film, whereas in the pore network its delivery is itself mixing-limited, so that a complete description would place the present diffusion-into-biofilm resistance in series with the pore-scale mixing resistance of the surrounding flow. Each of these extensions preserves the central result: in a porous medium, the rate that governs the system is not the intrinsic microbial rate but the rate at which substrate can be delivered to the cells.

5. Conclusions

We set out to determine how strongly diffusion into a biofilm reduces the microbial rate that a continuum model should use, and to put that reduction in a form a model can apply. The answer is a single effectiveness factor, controlled by one dimensionless group, that multiplies the laboratory rate. Its main lesson is interpretive: in a porous medium the Monod parameters a model carries are not pure properties of the cells. Wherever diffusion limits the supply of substrate, the apparent half-saturation constant is inflated and the apparent reaction order is pushed toward one-half, so a rate constant fitted to a biofilm or aggregate is in part a measure of its size and the flow around it. The practical takeaway is simple: form the Thiele modulus from the biofilm thickness, the diffusivity, and the laboratory constants, and when it approaches or exceeds one, replace the intrinsic Monod rate with the effectiveness-factor expression; otherwise the laboratory rate is safe to use. The treatment also has clear limits that point to the next steps. It assumes a single limiting substrate, a uniform flat layer of fixed thickness, and a substrate that is conservative outside the film, whereas many sediment processes, the anaerobic oxidation of methane among them, involve two co-diffusing substrates, curved and growing aggregates, and a supply that is itself mixing-limited; each of these turns the single factor into a richer but still tractable extension. The central message nonetheless holds: in the subsurface the rate that governs a reaction is set not by the cells alone but by how fast substrate reaches them, and that rate is now something a model can compute.

Code availability

All computations are implemented in Python. The code that produces the results and figures of this study is available from the corresponding author and will be sent by email on request.

Data availability

No measured data were generated or used in this study. The data underlying the figures and tables are available from the corresponding author and will be sent by email on request.

Author contributions

SA designed the study, carried out the derivations and computations, produced the figures, and wrote the manuscript.

Competing interests

The author declares that he has no conflict of interest.

Acknowledgements

During the preparation of this manuscript the author used a large language model to assist with editing text. The author reviewed and verified all content, results, and figures, and takes full responsibility for the work.

References

Aris, R. (1975). The Mathematical Theory of Diffusion and Reaction in Permeable Catalysts. Clarendon Press, Oxford.

Battiato, I., Tartakovsky, D. M. (2011). Applicability regimes for macroscopic models of reactive transport in porous media. Journal of Contaminant Hydrology 120–121, 18–26.

Bischoff, K. B. (1965). Effectiveness factors for general reaction rate forms. AIChE Journal 11(2), 351–355.

Blunt, M. J., Bijeljic, B., Dong, H., Gharbi, O., Iglauer, S., Mostaghimi, P., Paluszny, A., Pentland, C. (2013). Pore-scale imaging and modelling. Advances in Water Resources 51, 197–216.

Boetius, A., Ravenschlag, K., Schubert, C. J., Rickert, D., Widdel, F., Gieseke, A., Amann, R., Jorgensen, B. B., Witte, U., Pfannkuche, O. (2000). A marine microbial consortium apparently mediating anaerobic oxidation of methane. Nature 407, 623-626.

Dale, A. W., Regnier, P., Knab, N. J., Jorgensen, B. B., Van Cappellen, P. (2008). Anaerobic oxidation of methane (AOM) in marine sediments from the Skagerrak (Denmark): II. Reaction-transport modeling. Geochimica et Cosmochimica Acta 72, 2880-2894.

de Anna, P., Jiménez-Martínez, J., Tabuteau, H., Turuban, R., Le Borgne, T., Derrien, M., Méheust, Y. (2014). Mixing and reaction kinetics in porous media: an experimental pore-scale quantification. Environmental Science & Technology 48(1), 508–516.

573 Dentz, M., Le Borgne, T., Englert, A., Bijeljic, B. (2011). Mixing, spreading and reaction in
574 heterogeneous media: a brief review. Journal of Contaminant Hydrology 120–121, 1–17.

575 Dykaar, B. B., Kitanidis, P. K. (1996). Macrotransport of a biologically reacting solute
576 through porous media. Water Resources Research 32(2), 307–320.

577 Engasser, J.-M., Horvath, C. (1973). Effect of internal diffusion in heterogeneous enzyme
578 systems: evaluation of true kinetic parameters and substrate diffusivity. Journal of
579 Theoretical Biology 42, 137-155.

580 Goldstein, L. (1976). Kinetic behavior of immobilized enzyme systems. Methods in
581 Enzymology 44, 397-443.

582 Harremoës, P. (1978). Biofilm kinetics. In: Mitchell, R. (Ed.), Water Pollution Microbiology,
583 Vol. 2. Wiley, New York, pp. 71–109.

584 Monod, J. (1949). The growth of bacterial cultures. Annual Review of Microbiology 3, 371–
585 394.

586 Nauhaus, K., Albrecht, M., Elvert, M., Boetius, A., Widdel, F. (2007). In vitro cell growth of
587 marine archaeal-bacterial consortia during anaerobic oxidation of methane with sulfate.
588 Environmental Microbiology 9, 187-196.

589 Orcutt, B., Meile, C. (2008). Constraints on mechanisms and rates of anaerobic oxidation of
590 methane by microbial consortia: process-based modeling of ANME-2 archaea and sulfate
591 reducing bacteria interactions. Biogeosciences 5, 1587-1599.

592 Rittmann, B. E., McCarty, P. L. (1980). Model of steady-state biofilm kinetics. Biotechnology
593 and Bioengineering 22(11), 2343–2357.

594 Thiele, E. W. (1939). Relation between catalytic activity and size of particle. Industrial &
595 Engineering Chemistry 31(7), 916–920.

596 Williamson, K., McCarty, P. L. (1976). A model of substrate utilization by bacterial films.
597 Journal of the Water Pollution Control Federation 48(1), 9–24.

598 Wood, B. D., Whitaker, S. (1998). Diffusion and reaction in biofilms. Chemical Engineering
599 Science 53(3), 397–425.

600

Appendix A. Proof of the main-text equations

This appendix proves, with full intermediate steps and in the notation of the main text, the thirteen displayed equations (1)–(13). Symbols: S(z) is the local substrate concentration at depth z; D_e the effective diffusivity; R(S) the volumetric uptake; q_max the maximum specific uptake rate and X the biomass density, so r_max = q_max X is the maximum volumetric rate; K_s the half-saturation constant; L_f the film thickness; S_b the pore-water concentration at the surface; s_w the concentration at the grain wall; a_v the biofilm surface area per unit volume. Dimensionless variables are s = S/K_s, β = S_b/K_s, ζ = z/L_f, with the surface at ζ = 0 and the wall at ζ = 1, and a prime denotes d/dζ.

A.1 Monod rate and steady balance: Equations (1) and (2)

Equation (1) is the Monod volumetric uptake, the maximum volumetric rate r_max = q_max X times the saturating factor S/(K_s+S):

$$R(S) = r_{\max}\,\frac{S}{K_s + S}, \qquad r_{\max} = q_{\max} X$$

Equation (2) is the steady balance. The diffusive flux is −D_e dS/dz; at steady state its divergence equals the local consumption, so

$$\frac{d}{dz}\left(-D_e \frac{dS}{dz}\right) = -R(S)$$

with the surface value S(0) = S_b and no flux at the wall, dS/dz = 0 at z = L_f. That is Equation (2):

$$D_e \frac{d^2 S}{dz^2} = r_{\max}\frac{S}{K_s + S}, \qquad S(0) = S_b, \quad \left.\frac{dS}{dz}\right|_{z=L_f} = 0$$

A.2 Dimensionless form and Thiele modulus: Equations (3) and (4)

Introduce the scalings

$$s = \frac{S}{K_s}, \qquad \beta = \frac{S_b}{K_s}, \qquad \zeta = \frac{z}{L_f}$$

so that $d^2S/dz^2 = (K_s/L_f^2)\, s''$ and R(S) = r_max s/(1+s). Substituting into Equation (2),

$$\frac{D_e K_s}{L_f^2}\, s'' = r_{\max}\frac{s}{1+s}$$

Dividing by D_e K_s/L_f² collects every parameter into one group and gives Equation (3), with the surface and wall conditions carried over:

$$s'' = \phi^2\,\frac{s}{1+s}, \qquad s(0) = \beta, \quad s'(1) = 0$$

The single parameter is the Thiele modulus, Equation (4), the square root of the Damköhler number Da that compares the diffusion time L_f^2/D_e with the reaction time K_s/r_max:

$$\phi = L_f \sqrt{\frac{r_{\max}}{K_s D_e}} = \sqrt{\mathrm{Da}}, \qquad \mathrm{Da} = \frac{L_f^2/D_e}{K_s/r_{\max}}$$

A.3 Effectiveness factor, definition: Equation (5)

Equation (5) defines η as the uptake the film realizes divided by the uptake it would realize if every cell saw the surface concentration S_b (for which s/(1+s) = β/(1+β) everywhere):

$$\eta = \frac{\int_0^1 \frac{s}{1+s}\, d\zeta}{\beta/(1+\beta)}$$

A.4 Integrating the governing equation once: Equation (6)

Because ζ is absent from Equation (3), multiply both sides by s′: Here s' denotes ds/dzeta, the dimensionless concentration gradient, and s'' its second derivative.

$$s''\, s' = \phi^2\, \frac{s}{1+s}\, s'$$

The left side is an exact derivative by the chain rule,

$$\frac{d}{d\zeta}\left(\frac{1}{2}\, s'^2\right) = \phi^2\, \frac{s}{1+s}\, s'$$

and the right side becomes exact through the potential G, whose derivative is the Monod term: Here G(s) is the first-integral potential, defined so that its derivative G'(s) equals the local dimensionless uptake s/(1+s).

$$G(s) = s - \ln(1+s), \qquad G'(s) = \frac{s}{1+s}$$

$$\frac{d}{d\zeta}\left(\frac{1}{2}\, s'^2\right) = \phi^2\, \frac{dG}{d\zeta}$$

Equating the two and integrating inward from the wall (ζ = 1, where s = s_w and s′ = 0) gives

$$\frac{1}{2}\, s'^2 = \phi^2\, [\, G(s) - G(s_w)\,]$$

which, written for the gradient, is Equation (6):

$$|s'| = \phi \sqrt{2\, [\, G(s) - G(s_w)\,]}$$

A.5 Effectiveness factor, explicit form: Equation (7)

Since s″ equals φ^2 times the Monod term, the realized uptake telescopes to the surface slope (the flux entering the film at ζ = 0):

$$\int_0^1 \frac{s}{1+s}\, d\zeta = \frac{|s'(0)|}{\phi^2} = \frac{\sqrt{2\,[\,G(\beta) - G(s_w)\,]}}{\phi}$$

Dividing this by the reference uptake $\varphi^2 \cdot \beta/(1+\beta)$ of Equation (5) gives Equation (7):

$$\eta = \frac{\sqrt{2\,[\,G(\beta) - G(s_w)\,]}\,(1+\beta)}{\phi\,\beta}$$

A.6 Thickness condition for the wall concentration: Equation (8)

Separating Equation (6) as $d\zeta = -ds\,/(\varphi\sqrt{(2[G(s)-G(s\_w)])})$ and integrating across the film (ζ: 0→1 as s: β→s_w) turns the unit thickness into Equation (8), which fixes s_w:

$$\int_{s_w}^{\beta} \frac{ds}{\sqrt{2\,[\,G(s) - G(s_w)\,]}} = \phi$$

that is,

$$\int_{s_w}^{\beta} \frac{ds}{\sqrt{2\,[(s - \ln(1+s)) - (s_w - \ln(1+s_w))]}} = \phi$$

A.7 First-order limit: Equation (9)

For $\beta \ll 1$ the substrate is dilute, $s/(1+s) \approx s$, and Equation (3) linearizes; the solution meeting $s(0)=\beta$ and $s'(1)=0$ is a hyperbolic cosine centred on the wall:

$$s(\zeta) = \beta\,\frac{\cosh[\phi(1-\zeta)]}{\cosh\phi}$$

Its surface slope divided by the dilute reference uptake $\varphi^2\beta$ gives Equation (9), the classical Thiele slab result,

$$\eta = \frac{\tanh\phi}{\phi}$$

A.8 Partial-penetration limit: Equation (10)

For $\beta \gg 1$ the kinetics are zero order, $s/(1+s) \approx 1$, so $s'' = \varphi^2$; with the substrate exhausted in the interior the integrated equation gives the surface slope, and dividing by the zero-order reference uptake φ^2 gives Equation (10):

$$\eta \simeq \frac{\sqrt{2\beta}}{\phi}$$

valid once $\varphi > \sqrt{(2\beta)}$, the threshold at which the substrate no longer reaches the wall.

A.9 Deep-biofilm flux: Equation (11)

For a film much thicker than the penetration depth, $s\_w \to 0$. The dimensional surface flux follows from the integrated equation ($S = K\_s\, s$, $z = L\_f\, \zeta$): Here J is the dimensional flux

entering the film per unit surface area, and the limit s_w to zero expresses that the substrate is exhausted before it reaches the wall.

$$J = -D_e \left.\frac{dS}{dz}\right|_0 = \frac{D_e K_s}{L_f}\,|s'(0)| = \frac{D_e K_s}{L_f}\,\phi\sqrt{2\,G(\beta)}$$

Using φ/L_f = √(r_max/(K_s D_e)) to clear the thickness and K_s G(β) = S_b − K_s ln(1+S_b/K_s) gives Equation (11), the deep-film flux J:

$$J = \sqrt{2 D_e r_{\max}\,[\,S_b - K_s \ln(1 + S_b/K_s)\,]}$$

A.10 Apparent reaction order: Equation (12)

Equation (12) is the logarithmic slope of J against S_b. Writing J = √(2 D_e r_max G̃),

$$J = \sqrt{2 D_e r_{\max}\,\tilde{G}}, \qquad \tilde{G} = S_b - K_s \ln\left(1 + \frac{S_b}{K_s}\right)$$

the derivative of the bracket is

$$\frac{d\tilde{G}}{dS_b} = 1 - \frac{1}{1 + S_b/K_s} = \frac{S_b}{K_s + S_b}$$

and substituting gives Equation (12),

$$n_{\text{app}} = \frac{d\ln J}{d\ln S_b} = \frac{1}{2}\,\frac{S_b}{\tilde{G}}\,\frac{S_b}{K_s + S_b}$$

which runs continuously between the two limits,

$$n_{\text{app}} \to 1 \;\; (S_b \ll K_s), \qquad n_{\text{app}} \to \frac{1}{2} \;\; (S_b \gg K_s)$$

A.11 Upscaling to the pore network: Equation (13)

Equation (13) is the volumetric uptake a continuum model should use: the surface flux times the biofilm area density a_v, Here R_macro is the uptake per unit volume of porous medium and a_v the biofilm surface area per unit volume of that medium.

$$R_{\text{macro}} = a_v J = a_v \sqrt{2 D_e r_{\max}\,[\,S_b - K_s \ln(1 + S_b/K_s)\,]}$$

A.12 Generalized modulus used in the verification (Section 3.6)

The generalized modulus weights the rate by its own integral; for R̂(s) = s/(1+s) that integral is G(β), so Here Phi_g is the generalized modulus, R-hat(s) the dimensionless rate law and G(beta) its integral from zero to the surface saturation.

$$\Phi_g = \frac{\phi\, R(\beta)}{\sqrt{2\int_0^{\beta} R\; ds}} = \frac{\phi\,[\beta/(1+\beta)]}{\sqrt{2\,[\,\beta - \ln(1+\beta)\,]}}$$

against which the effectiveness factor collapses onto the universal curve $\eta\,\Phi_g \to 1$, which in the deep-film limit is an algebraic identity, as Section 3.6 explains.

Appendix B. Numerical code

The formulas above were verified against two independent numerical solutions of the same boundary-value problem: the first-integral quadrature used throughout, and a finite-difference Newton solver used for the validation figure. Both are reproduced here with inline comments; they require only NumPy. The potential is written G(s) and the dimensionless variables s, β, φ match Appendix A.

B.1 First-integral (semi-analytical) effectiveness factor

```
import numpy as np


# Dimensionless Monod biofilm:  s'' = phi^2 * s/(1+s),  s(0)=beta (surface),  s'(1)=0 (wall).
# G(s) is the first-integral potential, with G'(s) = s/(1+s) = the local dimensionless uptake.
G  = lambda s: s - np.log1p(s)        # G(s) = s - ln(1+s)
Gp = lambda s: s / (1.0 + s)          # G'(s) = local uptake rate


def thickness(s_w, beta, M=600):
    # Left side of the closure condition  int_{s_w}^{beta} ds / sqrt(2[G(s)-G(s_w)]) = phi  [Eq. 8].
    # Quadratic node spacing concentrates points near the integrable sqrt singularity at s = s_w.
    t    = np.linspace(0, 1, M)
    s    = s_w + (beta - s_w) * t**2              # map t in [0,1] -> s in [s_w, beta]
    dsdt = 2 * (beta - s_w) * t
    den  = np.sqrt(np.maximum(2 * (G(s) - G(s_w)), 1e-300))
    integ = dsdt / den
    integ[0] = np.sqrt(2 * (beta - s_w) / Gp(s_w)) if s_w > 0 else 0.0   # finite limit at s_w
    return np.trapezoid(integ, t)


def eta(phi, beta):
    # Solve thickness(s_w) = phi for the wall concentration s_w by bisection, then evaluate eta [Eq. 7].
    lo, hi = max(1e-7, 1e-7 * beta), beta * (1 - 1e-9)
    if thickness(lo, beta) < phi:                 # film deeper than full penetration -> s_w ~ 0
        s_w = lo
    else:
        for _ in range(70):                       # bracket s_w to ~21-digit precision
            mid = 0.5 * (lo + hi)
            if thickness(mid, beta) > phi: lo = mid
            else:                          hi = mid
        s_w = 0.5 * (lo + hi)
    # Effectiveness factor = realized surface flux / uptake evaluated at the surface concentration.
    return min(np.sqrt(2 * (G(beta) - G(s_w))) * (1 + beta) / (phi * beta), 1.0)
```

B.2 Independent finite-difference Newton solver (validation figure)

```
def eta_fd(phi, beta, N=300):
    # Fully independent finite-difference Newton solution of the SAME boundary-value problem [Eq. 3].
    # Node 0 is the surface (s = beta); node N is the grain wall (no-flux, s'(wall) = 0).
    h  = 1.0 / N
    s  = np.full(N + 1, 0.5 * beta + 1e-3); s[0] = beta
    f  = lambda x: x / (1 + x)                    # Monod uptake  s/(1+s)
    df = lambda x: 1.0 / (1 + x)**2               # its derivative (enters the Jacobian)
    for _ in range(60):                           # Newton iterations
        R = np.zeros(N)
        R[:-1] = (s[0:N-1] - 2*s[1:N] + s[2:N+1]) / h**2 - phi**2 * f(s[1:N])   # interior
        R[-1]  = (2*s[N-1] - 2*s[N]) / h**2       - phi**2 * f(s[N])            # no-flux wall
        diag  = -2.0 / h**2 - phi**2 * df(s[1:])
        upper = np.full(N - 1, 1.0 / h**2)
```

```
            lower = np.full(N - 1, 1.0 / h**2); lower[-1] = 2.0 / h**2   # mirror node sets s'(wall)=0
            J = np.diag(diag) + np.diag(upper, 1) + np.diag(lower, -1)
            delta = np.linalg.solve(J, -R)            # Newton update for the interior unknowns
            s[1:] = np.maximum(s[1:] + delta, 1e-12)
            if np.max(np.abs(delta)) < 1e-10: break
        zeta = np.linspace(0, 1, N + 1)
        return np.trapezoid(f(s), zeta) / f(beta)     # eta = mean uptake / surface uptake

# Agreement: max |eta_fd - eta| < 1e-3 over phi in [0.1, 100] and beta in [0.1, 100] (Figure 4).
```